Journal of Sound and Vibration 325 (2009) 609–628

Contents lists available at ScienceDirect

Journal of Sound and Vibration

journal homepage: www.elsevier.com/locate/jsvi

Vibration response of misaligned rotors

Tejas H. Patel [a], Ashish K. Darpe [b,*]

[a] Department of Mechanical Engineering, Charotar Institute of Technology, Changa 388421, India
[b] Department of Mechanical Engineering, Indian Institute of Technology, Delhi 110016, India

ARTICLE INFO

Article history:
Received 15 July 2008
Received in revised form
19 January 2009
Accepted 20 March 2009
Handling Editor: J. Lam
Available online 21 April 2009

ABSTRACT

Misalignment is one of the common faults observed in rotors. Effect of misalignment on vibration response of coupled rotors is investigated in the present study. The coupled rotor system is modelled using Timoshenko beam elements with all six dof. An experimental approach is proposed for the first time for determination of magnitude and harmonic nature of the misalignment excitation. Misalignment effect at coupling location of rotor FE model is simulated using nodal force vector. The force vector is found using misalignment coupling stiffness matrix, derived from experimental data and applied misalignment between the two rotors. Steady-state vibration response is studied for sub-critical speeds. Effect of the types of misalignment (parallel and angular) on the vibration behaviour of the coupled rotor is examined. Along with lateral vibrations, axial and torsional vibrations are also investigated and nature of the vibration response is also examined. It has been found that the misalignment couples vibrations in bending, longitudinal and torsional modes. Some diagnostic features in the fast Fourier transform (FFT) of torsional and longitudinal response related to parallel and angular misalignment have been revealed. Full spectra and orbit plots are effectively used to reveal the unique nature of misalignment fault leading to reliable misalignment diagnostic information, not clearly brought out by earlier studies.

© 2009 Elsevier Ltd. All rights reserved.

1. Introduction

After unbalance, misalignment is accepted as the second most commonly observed disturbance source in rotor systems. Misalignment is categorized in two types, (1) angular misalignment and (2) parallel misalignment. Even after using sophisticated alignment techniques like laser alignment, rotor system is likely to have some residual misalignment. Misalignment also develops over a period of continuous operation because of unequal foundation movement or uneven thermal heating in the rotor system. Thus, misaligned rotor condition always prevails in rotor systems; however, it may be within acceptable levels. Though researchers acknowledge the adverse effect of misalignment on the dynamic performance of the rotor system, relatively fewer studies have been conducted in this regard.

Misalignment of the machinery shafts generates reaction forces and moments at coupling location, which significantly affect the vibration behaviour of the rotors. Accurate prediction of vibration response of the misaligned rotor strongly depends on the realistic modelling of the misalignment effect. Gibbons [1] proposed formulation of misalignment forces the coupling. Later many researchers adopted force equations based on the analysis proposed by him. Sekhar and Prabhu [2] evaluated the effect of coupling misalignment on vibration response of the rotor. Based on simple misalignment model [3] they showed 2*X* vibration response as the misalignment vibration symptom. Xu and Marangoni [4] derived misalignment forces based on kinematics of the Hooke's joint. The derived equations indicate the forcing frequencies due

* Corresponding author.
E-mail address: akdarpe@mech.iitd.ac.in (A.K. Darpe).

0022-460X/$ - see front matter © 2009 Elsevier Ltd. All rights reserved.
doi:10.1016/j.jsv.2009.03.024

to shaft misalignment are even multiple frequencies of the motor rotational speed. On the other hand, Redmond and Al-Hussain [5,6] opined that the modelling of misaligned coupling using kinematics of Hooke's joint is not appropriate for all types of flexible couplings, as orthogonality between driven and driver hub rotation vectors is not possible for other types of couplings. They modelled mechanical coupling in the form of a radially rigid, pinned joint with rotational stiffness and found 1*X* bending–torsional coupled vibration response for the rotor with parallel misalignment. Cantania and Maggiore [7] also emphasized the inadequacy of the Hooke's joint kinematics approach for all practical misalignment conditions. Recently, Lees [8] studied the effect of parallel misalignment in rigidly coupled rotors. Kinematics of the connecting bolts of a three-pin coupling was proposed. Vibrations at twice the rotor speed due to presence of misalignment are observed.

From the literature cited above, it may be noted that most of the previous studies have considered different kinematics of the mechanical couplings under misalignment condition. This could be the major reason behind discrepancies found in harmonics generated due to misalignment. For example, vibrations at twice the rotational speed (i.e. 2*X*) and its harmonics are reported [4,9] as a characteristic misalignment feature. Contrary to this, Redmond and Al-Hussain [6] reported coupled lateral–torsional 1*X* vibrations for parallel misalignment. It is also reported [10] that different types of flexible couplings reveal different frequency composition in the vibration response due to misalignment. Hence, the generalization of misalignment vibration signature based on any one of these studies is not appropriate. Vibration with strong 2*X* harmonic is the widely accepted misalignment vibration signature among practicing engineers. However, there are other faults, such as fatigue crack, stiffness asymmetry, etc. also generate strong 2*X* vibrations. There is no clear and convincing distinction among these faults, available in the literature. In practice any signs of 2*X* frequency component might lead to confusing picture from the diagnostic point of view. The situation thus suggests need of a well-defined misalignment diagnosis strategy.

When two shafts misalign, a fixed amount of relative displacement between the coupling faces is imposed. This relative offset between the coupling faces introduces preload forces on the connected shafts, and subsequently on the bearings and other elements of the rotors. Along with the preload, there are misalignment excitations varying with the shaft rotation, the exact nature of which primarily depends on the constructional features of the coupling. More importantly, these varying components of misalignment excitation influence the vibration response of misaligned rotors. It may also be noted that the flexible elements in the coupling flex with shaft rotation, which allows the flexible coupling to accommodate certain level of the misalignment prevailing in the system. In fact, the actual level of the misalignment is varying with the shaft rotation. It is necessary to consider both these aspects in a model, while estimating the misalignment effect.

There is a wide variety of commercially available flexible couplings. Depending upon construction and type of flexible elements used, these couplings demonstrates different kinematics in operation that is often difficult to formulate mathematically. Except universal joint, kinematics relations of the other types of couplings are not studied for the misalignment conditions. Due to the complexities involved, most practical approach to obtain exact harmonic composition and level of misalignment forces and moments is to find the misalignment forces experimentally.

Based on the experimental examination on force–displacement relations for different types of couplings, Saavedra and Ramirez [11] proposed a coupling stiffness matrix and used it in the FEA of a misaligned rotor system. However, the derived stiffness coefficients vary with shaft rotation even in absence of misalignment. In addition, the important torsional dof was not considered and bending–axial coupling was also not evident. The present study outlines a method of determination of the misalignment excitation, wherein a coupled rotor bearing system with pin-bush flexible coupling is investigated. Misalignment forces and moments are obtained experimentally using a 6-axis load-cell. The measurement of all the six forces and moments are used to formulate a more refined and realistic coupling stiffness matrix (with all the six dof) than that in Ref. [11]. The model proposed in this paper considers six dof with all possible motion coupling, i.e. bending–axial–torsional. Effect of parallel and angular misalignments on the vibration response of the coupled rotors is studied. Steady-state vibration response is obtained at various sub-critical rotor speeds.

It may be noted that the conventional spectral analysis using fast Fourier transform (FFT) algorithm treats rotor vibration signal as a real quantity and hence the corresponding frequency spectrum loses important rotor orbital information such as directivity, i.e. forward and backward whirl of vibratory motion. Full spectrum overcomes this limitation by retaining the relative phase information between two measured vibration signals [12]. This attribute makes the full spectrum one of the important diagnostic tools and there have been research studies [13,14] that report its effectiveness for rotating machine fault detection. In the present study, use of full spectrum to identify specific misalignment fault features is explored.

2. Formulation of misalignment effect in finite element model

Fig. 1a show the experimental set-up used to ascertain the misalignment induced forces and moments. The set-up consists of a rotor (rotor-1) supported on rolling element bearings. On the extreme right, Fig. 1a also shows a second short rotor (rotor-2) that is mounted on a 6-axis load-cell via bearing housing and a circular seat. The two rotors are coupled through a pin-bush (three-pin) type flexible coupling. The 6-axis load-cell can simultaneously measure forces and moments along all three axes (i.e. F_x, F_y, F_z, M_x, M_y and M_z). Reference coordinate axes are shown in Fig. 1a. Beneath the load-cell, an arrangement is made to induce misalignment using pre-machined shims of fixed thickness. The close-up view of the coupling that could be seen partially hidden behind the probe holder in Fig. 1a is shown in Fig. 1b. The four eddy current proximity probes (one each in horizontal and vertical directions) are mounted above the machined surfaces of the

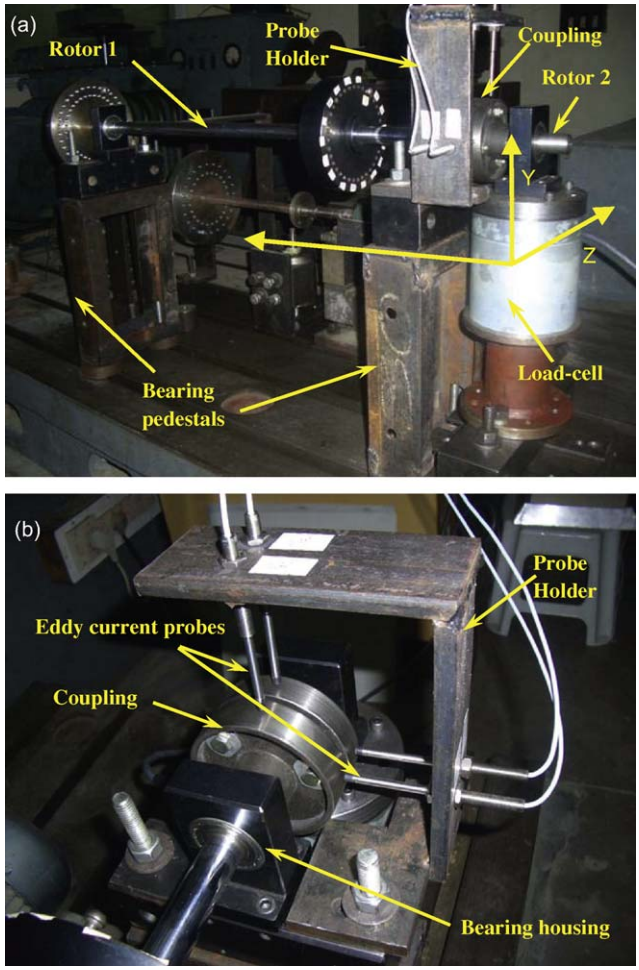

Fig. 1. Set-up for measurement of misalignment excitation: (a) full view of the arrangement and (b) a close-up view showing probe locations on coupling surfaces.

metallic flexible coupling halves. These probes measure gap between the coupling surface and the probe tip, which in turn is utilized to calculate the exact amount of misalignment induced between the two rotors.

Before connecting the coupling halves to each other, misalignment between two shafts is brought to a minimum possible level. This condition with residual misalignment is taken as base-line case. The rotor shaft is now gradually rotated and simultaneous measurement of forces as well as moments for this base-line case is done using the load-cell. These measured forces and moments are considered as reference values for subsequent calculation of misaligned coupling stiffness matrix. All the experimentally measured forces and moments variation (i.e. F_x, F_y, F_z, M_x, M_y and M_z) are curve fitted using a high order polynomial fit. The waveforms of these forces and moments for the initial residual misalignment case are shown in Fig. 2.

The coupling halves are now subjected to either angular misalignment or parallel misalignment. For angular misalignment, the axis of the shaft is inclined relative to the other shaft in horizontal plane by suitably moving the load-cell pedestal while the proximity probes tracked the actual angle induced. On the other hand, parallel misalignment can be conveniently introduced by inserting pre-machined shims of defined thickness beneath the load-cell. Once the probe readings confirm the type and amount of misalignment induced in the system, the rotor shaft is rotated gradually and measurement of forces and moments is done in the way it was done for the base-line case. Fig. 3a shows the misalignment excitations due to parallel misalignment along vertical direction (i.e. $dy = 1.5$ mm). Misalignment forces and moments are also measured for the angular misalignment (Fig. 3b) about vertical coordinate axis ($\alpha = 1.5^\circ$; i.e. angular misalignment in horizontal plane). Comparison of Figs 2 and 3 clearly shows the differences in level and variation of measured forces and moments with shaft rotation. It is clear that the force and moment variation for the base-line case is mainly once in one cycle of shaft rotation (i.e. 1X). Fig. 3 not only indicates high level of forces and moments associated with misalignment but also reveal higher order frequencies.

Using the magnitude of induced misalignment and differences in the measured forces and moments for misaligned and base-line cases, stiffness coefficients are calculated (Fig. 4). To illustrate one sample calculation, let us take the induced misalignment is 'dy' and the measured forces and moments (obtained after compensating the residual or base-line data) are dF_x, dF_y, dF_z, dM_x, dM_y and dM_z. Now the misalignment stiffness coefficients are calculated as $k_{xy} = dF_x/dy$, $k_{yy} = dF_y/dy$,

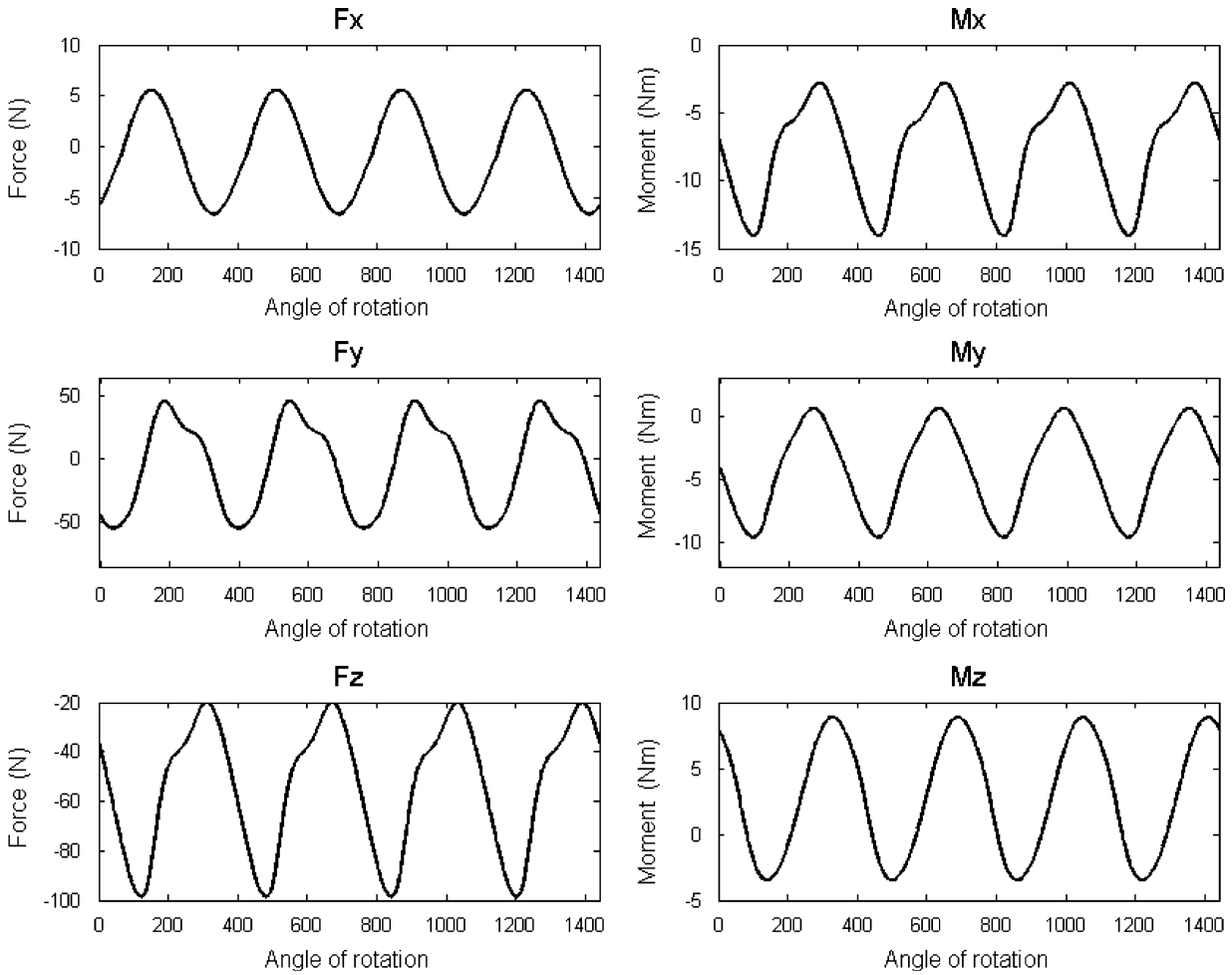

Fig. 2. Force and moment measurement for rotors with residual misalignment.

$k_{zy} = \mathrm{d}F_z/\mathrm{d}y$, $k_{\phi xy} = \mathrm{d}M_x/\mathrm{d}y$, $k_{\phi yy} = \mathrm{d}M_y/\mathrm{d}y$ and $k_{\phi zy} = \mathrm{d}M_z/\mathrm{d}y$. The stiffness coefficients for other type and direction of misalignment are similarly calculated. The stiffness coefficients thus found forms the coupling stiffness matrix for misaligned coupling halves. Once the exact level of induced misalignment is known the corresponding misalignment excitation acting at the coupling location in the FE model of coupled rotor system can be obtained by multiplying the coupling stiffness matrix with misalignment displacement vector (discussed later in Section 3.2). As the induced forces change as a function or rotation, so does the stiffness matrix terms and in turn the misalignment excitation acting at the coupling locations, which are finally the source of peculiar frequency composition of vibration response of misaligned rotors. Eq. (1) gives the coupling stiffness matrix. The cross-stiffness terms are $k_{xy} = k_{yx}$, $k_{xz} = k_{zx}$, $k_{\phi_z x} = k_{x\phi_z}$ and $k_{\phi_y x} = k_{x\phi_y}$. The coupling stiffness matrix can thus be written as

$$[\mathbf{K}^c]_{12\times12} = \begin{bmatrix} [\mathbf{K}]_{6\times6} & [\mathbf{0}]_{6\times6} \\ [\mathbf{0}]_{6\times6} & [\mathbf{K}]_{6\times6} \end{bmatrix} \tag{1}$$

where

$$[\mathbf{K}]_{6\times6} = \begin{bmatrix} 0 & k_{yx} & k_{xz} & 0 & k_{\phi_z x} & k_{\phi_y x} \\ k_{xy} & k_{yy} & k_{zy} & k_{\phi_x y} & k_{\phi_y y} & k_{\phi_z y} \\ k_{xz} & k_{yz} & k_{zz} & k_{\phi_x z} & k_{\phi_y z} & k_{\phi_z z} \\ 0 & k_{y\phi_x} & k_{z\phi_x} & 0 & k_{\phi_z\phi_x} & k_{\phi_y\phi_x} \\ k_{x\phi_z} & k_{y\phi_z} & k_{z\phi_z} & k_{\phi_x\phi_z} & k_{\phi_y\phi_z} & k_{\phi_z\phi_z} \\ k_{x\phi_y} & k_{y\phi_y} & k_{z\phi_y} & k_{\phi_x\phi_y} & k_{\phi_y\phi_y} & k_{\phi_z\phi_y} \end{bmatrix} \tag{2}$$

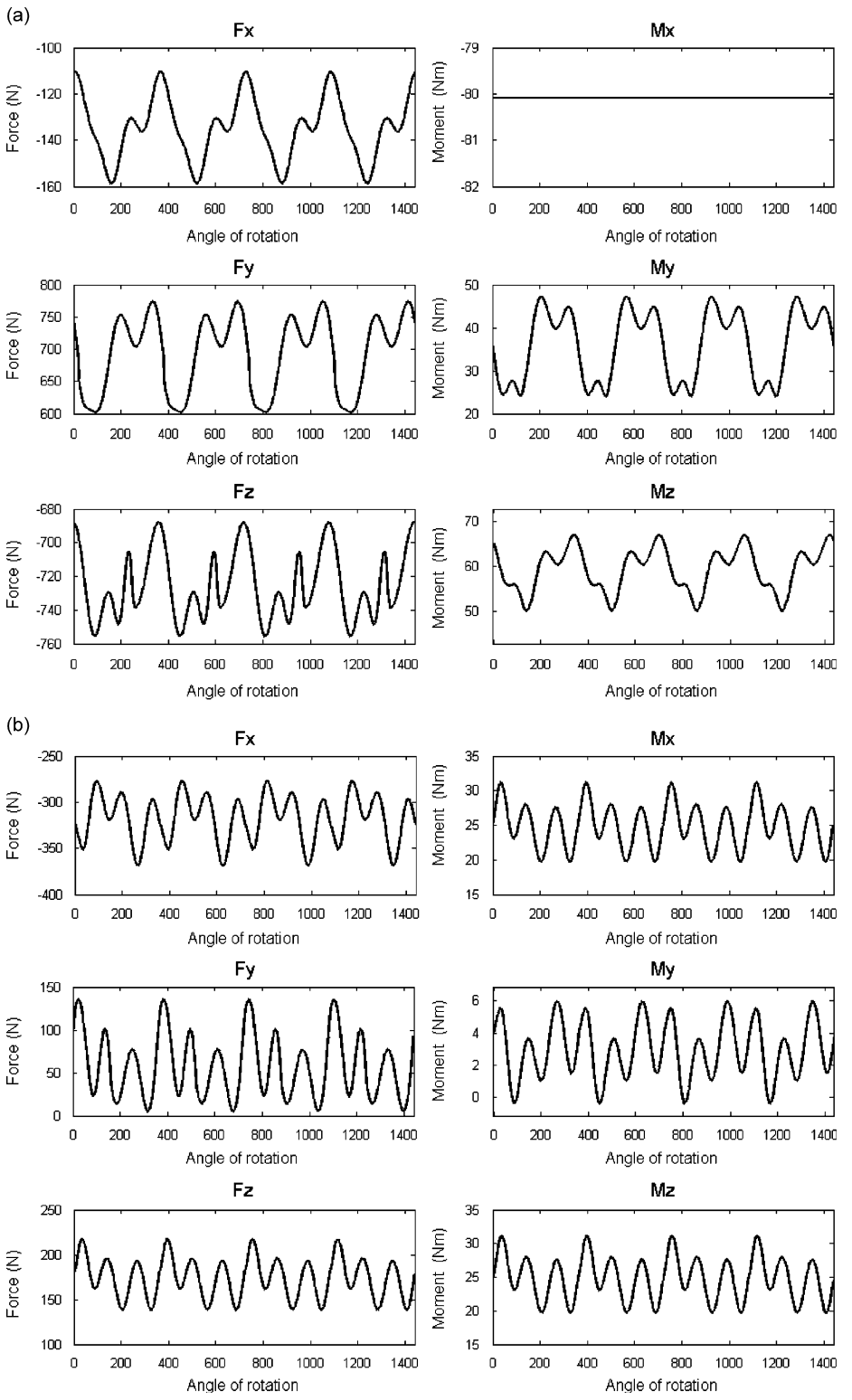

Fig. 3. Misalignment force and moment variation with shaft rotation angle for: (a) parallel misalignment and (b) angular misalignment.

Presence of one or more terms of the matrix depends upon the type and direction of misalignment present in the system. For example, if misalignment in Y direction (i.e. dy) is zero, then, terms $k_{xy} = k_{yy} = k_{zy} = k_{\phi xy} = k_{\phi yy} = k_{\phi zy} = 0$.

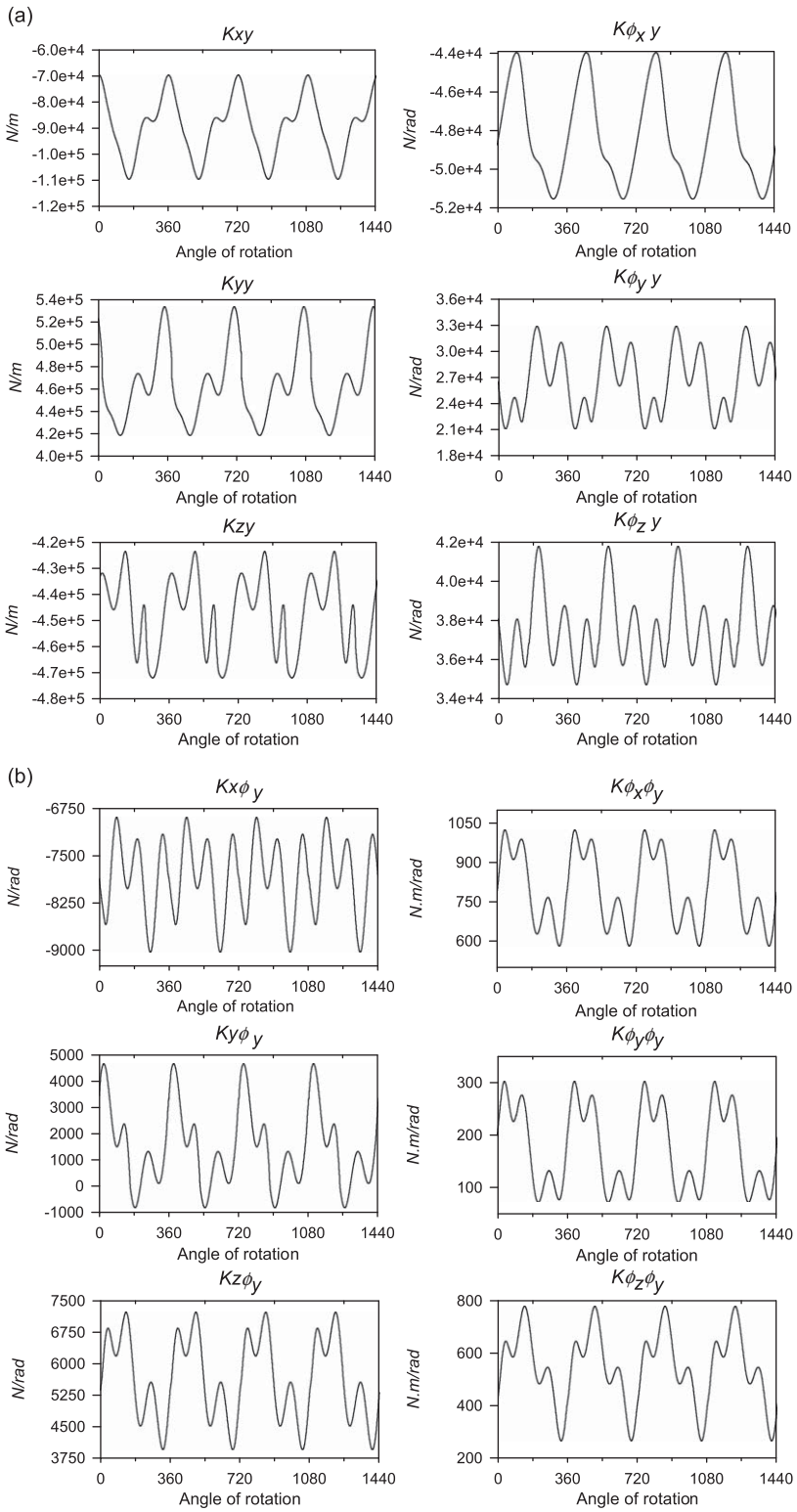

Fig. 4. Variation in stiffness coefficients with shaft rotation angle for: (a) parallel misalignment and (b) angular misalignment.

The forces induced on the coupling location due to the misalignment in the coupling halves can be estimated by multiplying the coupling stiffness matrix discussed above with the misalignment vector given by $\{\mathbf{q}_{mis}\} = \{0\ dy\ dz\ 0\ \alpha\ \beta\}$, Where, d$y$ and dz are parallel misalignment values along Y- and Z-axes, respectively, and α and β are the angular

misalignments about *Y*- and *Z*-axes, respectively (Fig. 1). It may be noted that the derived stiffness matrix given by Eq. (2) does not become part of the FE assemblage of the rotor bearing system. Instead the effect of misaligned coupling on the coupled rotor bearing system is accounted by applying external forces acting at the FE node corresponding to the coupling location (discussed in detail in Section 3.2). These external forces are function of rotor angular position and are dependent coupling stiffness matrix and the induced misalignment.

Fast Fourier transform of the variation of stiffness coefficients during a rotor rotation and harmonics of the stiffness variation is obtained (Fig. 5). Although many harmonics are present in the FFT plots of stiffness coefficients, 1*X* and 3*X* are the strongest spectral components. The phase information of these harmonics is also recorded. The stronger amplitude of 3*X* harmonic is due to pulling action of three pins of the coupling during a rotation. Misalignment excitation thus calculated (i.e. considering harmonics and phase information) is used as applied forces for calculation of the dynamic response of the misaligned coupled rotors. Since the misalignment forces and moments generated with shaft rotation take care of the type of misalignment as well as the coupling kinematics, the misalignment excitations accurately predicts the exact dynamic forces generated during shaft rotation in the misaligned rotors.

3. Equations of motion of misaligned coupled rotors

An investigation of the vibration characteristics of the misalignment fault is carried out using a finite element model of the coupled rotor system. Two identical rotors are coupled with each other via flexible coupling (Fig. 6a). The misalignment is considered between two rotor shafts across the coupling halves. The shafts of diameter *D* are supported on the rigid supports with span length of *L*. Discs of mass *m* are placed at the central span on both the shafts.

3.1. Equations of motion

The generalized form of the equations of motion using Timoshenko beam element can be written as

$$[\mathbf{M}]\{\ddot{\mathbf{q}}\} + [\mathbf{C}]\{\dot{\mathbf{q}}\} - \omega[\mathbf{G}]\{\dot{\mathbf{q}}\} + [\mathbf{K}]\{\mathbf{q}\} = \{\mathbf{F}\} \tag{3}$$

where [**M**], [**C**], [**G**] and [**K**] are the mass, damping, gyroscopic and stiffness matrices, respectively. {**F**} is the external excitation force vector due to unbalance and misalignment, $\{\mathbf{q}_i\} = \{X_i\ Y_i\ Z_i\ \theta_{xi}\ \theta_{yi}\ \theta_{zi}\}$, is the generalized coordinate of the system, where *i* is the node number and ω the rotational speed.

Figs. 6a and b show the schematic of the coupled rotor system along with its finite element model. Timoshenko beam elements with six dof per node are considered for FE modelling of the system. The model would thus be useful to study possible coupling of vibration among these dof due to presence of misalignment. The coupled rotors are discretized into 33 elements with 14 elements for each rotor and 5 elements between the rotor support bearings as shown in Fig. 6b. The coupling halves are modelled as nodes of the central element (element no. 17). The discs and coupling halves inertias (i.e. translational and rotational both) are lumped at their respective node locations. The time varying forces, which are dependent on the misalignment coupling stiffness matrix and the misalignment vector (given by Eq. (5) later in Section 3.2), are applied at these nodes to account for the misalignment induced between the coupling halves. Thus, in absence of any misalignment, the forces applied at the coupling node are zero; however, the mass and inertia of the coupling continue to be a part of the FE model. Thus, the stiffness matrix of Eq. (1) does not explicitly become part of the FE model of the rotor.

3.2. Calculation of misalignment forces and moments

The misaligned force vector estimated using the stiffness matrix for the coupling (formulated using the experimental measurement of forces and moments) is applied to the rotor at the coupling location. However, the difference in the coordinates due to misalignment between the coupling halves has to be accounted before applying misalignment forces and moments.

Fig. 6c shows the schematic of misaligned coupling halves. To understand coupling misalignment effect; two sub-coordinates ($X_1Y_1Z_1$ and $X_2Y_2Z_2$ for rotor-1 and rotor-2, respectively) associated with two different rotors are considered. As long as the rotors are aligned there is no difference in these coordinate systems. One coupling half is attached to rotor-1 and other coupling half to the rotor-2. So, the coordinates of the coupling nodes A and B, should be referred to $X_1Y_1Z_1$ and $X_2Y_2Z_2$ coordinate systems, respectively. Since the coupling halves are associated with different rotors, the problem here is to relate the misalignment forces and moments to the coupling nodes. While calculating the misalignment forces on rotor-1, the coupling nodes are referred to $X_1Y_1Z_1$ coordinate system. Similarly, for misalignment excitation on rotor-2, coupling nodes are referred to $X_2Y_2Z_2$ coordinate system [11]. The misalignment force–displacement relationship at the coupling location can be written as

$$\begin{aligned} \mathbf{K}_u^c\{\mathbf{q}_1^c\} &= \mathbf{F}_1^A; \\ \mathbf{K}_l^c\{\mathbf{q}_2^c\} &= \mathbf{F}_2^B \end{aligned} \tag{4}$$

where $\mathbf{K}_u^c$ and $\mathbf{K}_l^c$ are, respectively, the upper and lower half of the coupling stiffness matrix $\mathbf{K}^c$ (Eq. 1). The coupling stiffness matrix is made of misalignment stiffness coefficients derived as described in Section 2. Vectors $\{\mathbf{q}_1^c\}$ and $\{\mathbf{q}_2^c\}$ are

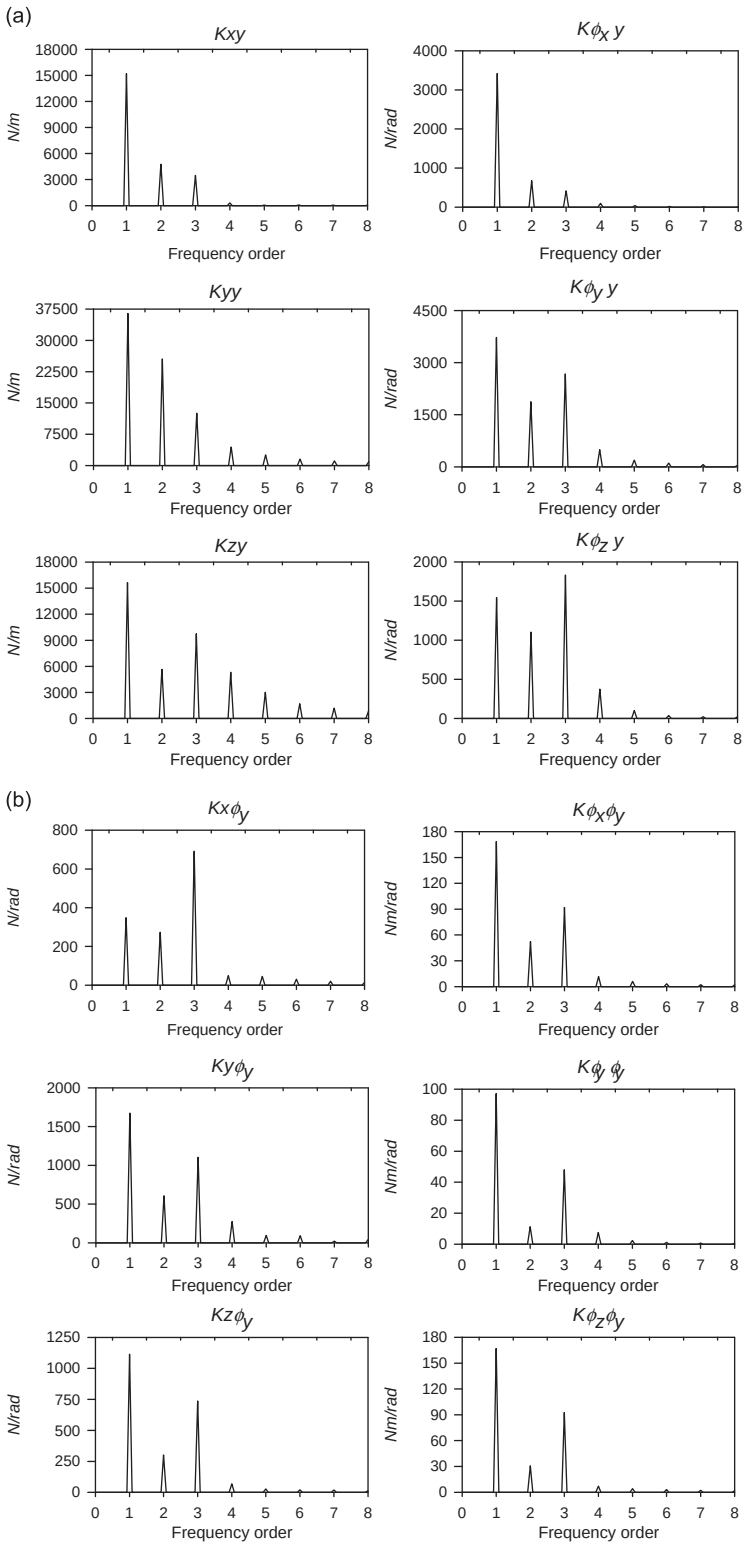

Fig. 5. FFT plots of misalignment stiffness coefficients for: (a) parallel misalignment and (b) angular misalignment.

coupling node displacements, which are 12×1 vectors. The subscripts 1 and 2 refer to the $X_1Y_1Z_1$ and $X_2Y_2Z_2$ coordinate systems, respectively. $\mathbf{F}_1^A$ and $\mathbf{F}_2^B$ are the misalignment force vectors at coupling nodes A and B, respectively. The vectors $\{\mathbf{q}_1^c\}$ and $\{\mathbf{q}_2^c\}$ are split in half; i.e. $\{\mathbf{q}_1^c\} = \{\mathbf{q}_1^A, \mathbf{q}_1^B\}$ and $\{\mathbf{q}_2^c\} = \{\mathbf{q}_2^A, \mathbf{q}_2^B\}$; where $\mathbf{q}_1^A$ and $\mathbf{q}_2^A$ are nodal displacement vectors at A in

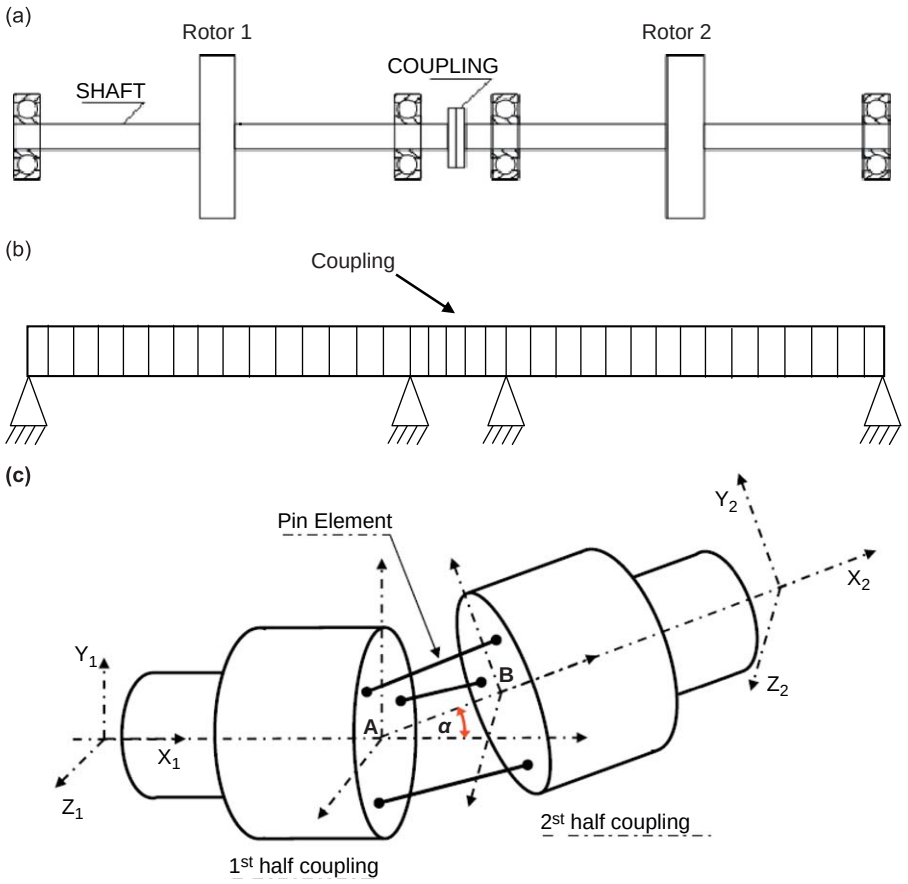

Fig. 6. (a) Coupled rotor system, (b) FE model of the system and (c) coupling halves and associated coordinate system in misalignment.

$X_1Y_1Z_1$ and $X_2Y_2Z_2$ coordinate systems; $\mathbf{q}_1^B$ and $\mathbf{q}_2^B$ are nodal displacement vectors at B in $X_1Y_1Z_1$ and $X_2Y_2Z_2$ coordinate systems.

Now, $\{\mathbf{q}_1^B\}$ and $\{\mathbf{q}_2^A\}$ can be referred to $X_2Y_2Z_2$ and $X_1Y_1Z_1$ systems, respectively, using a coordinate transformation matrix **T**.

$$\{\mathbf{q}_1^B\} = [\mathbf{T}]\{\mathbf{q}_2^B\} - \{\mathbf{q}_{mis}\};$$
$$\{\mathbf{q}_2^A\} = [\mathbf{T}]^{-1}\{\mathbf{q}_2^A\} + \{\mathbf{q}_{mis}\};$$

where

$$[\mathbf{T}] = \begin{bmatrix} 1 & 0 & 0 & 0 & 0 & 0 \\ 0 & \cos\theta & \sin\theta & 0 & 0 & 0 \\ 0 & -\sin\theta & \cos\theta & 0 & 0 & 0 \\ 0 & 0 & 0 & 1 & 0 & 0 \\ 0 & 0 & 0 & 0 & \cos\theta & \sin\theta \\ 0 & 0 & 0 & 0 & -\sin\theta & \cos\theta \end{bmatrix} \quad (5)$$

and $\{\mathbf{q}_{mis}\} = \{0\ dy\ dz\ 0\ \alpha\ \beta\}$ is the misalignment vector as mentioned earlier.

4. Vibration analysis of misaligned rotors

Vibration response of the two identical rotors (Fig. 6) connected by a three-pin flexible coupling is discussed in this section. Each rotor carries a central disc and is supported on simple rigid bearing supports. The physical system parameters considered for the analysis of the misaligned rotors are as follows: disc mass, $m = 6$ kg; disc area moment of inertia, $I_d = 12.14\text{E}{-}03\ \text{mm}^4$. Length of the shaft between bearing supports $= 0.7$ m. Distance between bearing supports near the coupling $= 0.25$ m (Fig. 6). Shaft diameter $= 25$ mm. The misalignment effect is considered in the form of external

excitation forces at the coupling's location. Mass/inertia of the flexible coupling considered in the study: mass, $m_c = 0.35$ kg; moment of inertia, $I_d = 5.0\text{E}{-}03$ mm^4. Unbalance eccentricity of 2.2E−05 m is considered. The coupled rotor system has following first few natural frequencies in various modes: bending: 49.64 and 56.24 Hz; torsional: 61.34 and 117.9 Hz; axial: 605 Hz.

Using the system parameters mentioned above, the equations of motion (Eq. (3)) are solved using Newmark integration method. The steady-state vibration response will be studied with and without misalignment. Proportional damping matrix is assumed here with $[\mathbf{C}] = \alpha_d[\mathbf{K}]+\beta_d[\mathbf{M}]$, where the constants α_d and β_d are found to be 0.8132 rad/s and 7.185E−5 s/rad, respectively, for the assumed modal damping ratios 0.01 and 0.05 for the first two modes. Steady-state vibration response is obtained for both the types of misalignment, i.e. parallel and angular misalignment. Speed range considered for the simulation work covers integer fraction of the first bending natural frequency (i.e. $\omega = \omega_n/2$, $\omega_n/3$, etc.), to examine the possible subharmonic resonances for the misaligned rotor system. Unbalance phase angles are considered to be zero on both the rotor discs in most of the simulations. In limited studies made in the past related to coupled vibrations due to misalignment, the studies have investigated either bending–torsional coupling [6] or bending–axial coupling [3]. Coupling phenomena, with possibility of coupling among all dof, i.e. lateral–torsional–axial is systematically investigated for the first time in the present study.

Although different signal processing techniques have evolved over the years, spectral analysis using FFT algorithm is the widely used technique for vibration analysis of the machines and structures. However, basic drawback with the FFT is that it treats vibration signal as real quantities; hence both $-nX$ and $+nX$ parts of the FFT are identical and only one half ($+nX$) is plotted. The frequency spectrum thus loses important orbital information such as directivity, i.e. forward or backward whirl. In the case of rotor vibrations, full spectrum overcomes this limitation by retaining the relative phase information between two measured vibration signals [12]. The full spectrum is based on the rotor vibration data from lateral directions (i.e. Y and Z), hence,$-nX$ and $+nX$ parts are not identical. In other words, it is the spectrum of an orbit [12]. At a glance, the full spectrum plot tells us whether the rotor orbit frequency components are forward or backward in whirl, in relation to the rotor spin direction. The process of obtaining a full spectrum and related mathematical background are detailed in Refs. [12–14]. In this paper, full spectrum analysis is attempted on misalignment vibration response with an objective of deriving misalignment vibration signature.

4.1. Unbalance vibration response of coupled rotors without misalignment

Lateral vibration response of the coupled rotors without any misalignment is first investigated to form a baseline case. As expected the coupled rotor exhibits synchronous vibration response; hence the time domain and FFT data for this case is not shown here. Fig. 7 shows the full spectrum plots of the vibration response of rotor-1 for the rotor speed equal to one-third and one-half of the first bending natural frequency (i.e. $\omega = \omega_n/3 = 16.534$ Hz and $\omega = \omega_n/2 = 24.8$ Hz). It may be noted that the vibration amplitude only along the positive frequency axis is present. The rotor motion is thus forward whirling in nature. This is a well-established fact that when unbalance is the only fault present in the system, the vibrations are synchronous and forward whirling. It may be noted that the vibration response of the second rotor is exactly the same as of first rotor; hence the full spectra of rotor-1 is shown. It may be further noted that the vibrations along longitudinal and torsional dof are zero, hence, are not shown here.

4.2. Unbalance vibration response of coupled rotors with parallel misalignment

In this section, vibration response of the coupled rotors due to parallel misalignment between the axes of the two rotors is investigated. Excitation forces and moments due to misalignment are considered at coupling location as discussed in the previous section. Parallel misalignment of 0.32 mm is considered along the Y direction (i.e. vertical) in the present study, i.e. $\mathrm{d}y = 0.32$ mm.

Fig. 8 shows the time waveforms and fast Fourier transforms of the vertical, horizontal, axial and torsional vibration responses of rotor-1 of the misaligned rotors ($\mathrm{d}y = 0.32$ mm), for rotational speed $\omega = \omega_n/4 = 12.4$ Hz, i.e. 1/4th of the speed corresponding to first bending natural frequency of the rotor. Vibration response along both the lateral directions (i.e. vertical and horizontal) shows harmonics of the rotational speed. In particular, the first four harmonics are clearly visible. It may be recalled from the Fourier spectrum plots (Fig. 5a) of stiffness coefficients associated with parallel misalignment, that the variation of stiffness coefficients exhibits harmonics of rotational speed, usually the first six out of which first four harmonics are significant. Maximum vibration amplitude is observed at 49.6 Hz frequency value. Since, the rotational speed is 12.4 Hz (i.e. $\omega_n/4$); the fourth harmonic of the rotational speed matches with the bending natural frequency (49.6 Hz) and rotor experiences subharmonic resonance. The induced misalignment along the vertical direction increases the vertical stiffness of the rotor system. This is manifested by decreased vibration level in the vertical direction compared to the vibrations in the horizontal direction.

The presence of axial and torsional responses despite of lack of explicit axial or torsional excitation is attributed to misalignment as the unbalanced aligned rotor does not experience vibrations along axial and torsional dof. However, the lateral–axial vibration coupling due to misalignment is weaker. The axial (Figs. 8e and f) and torsional (Figs. 8g and h) responses are strongly 1X with noticeable presence of 2X, 3X, etc. harmonic frequency components. The 5X component is

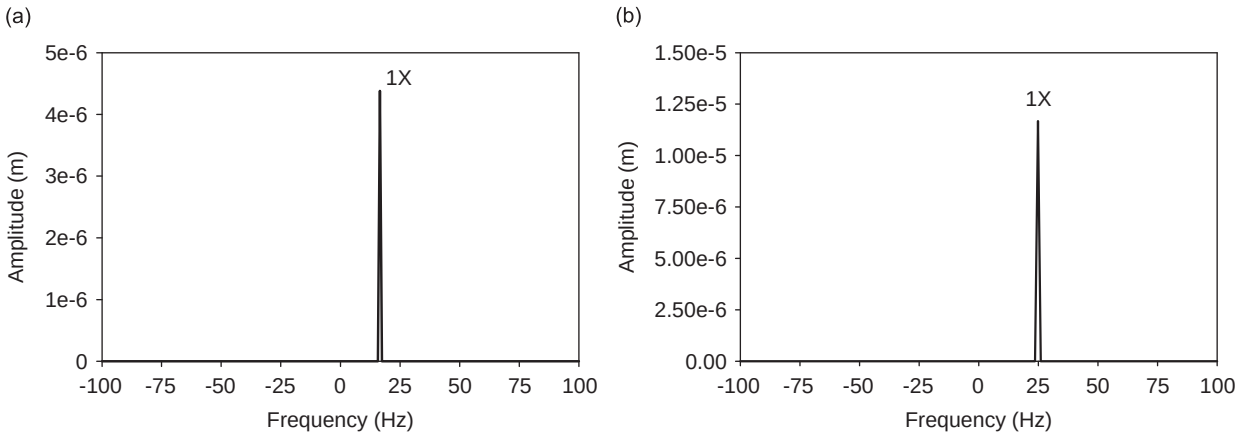

Fig. 7. Full spectra of unbalance vibration response of coupled rotor without misalignment: (a) $\omega = \omega_n/3 = 16.534$ Hz and (b) $\omega = \omega_n/2 = 24.8$ Hz.

observed stronger in comparison with other higher harmonics in the torsional response. This is due to the fact that the 5*X* frequency component (i.e. 62 Hz) is very close to the first torsional natural frequency (i.e. 61.3 Hz). It may also be noted that in absence of misalignment, horizontal vibration takes place about zero mean and vertical vibration takes place about the mean at static deflection. However, with misalignment in the system, the shift in mean value from its usual zero value is observed for horizontal, axial and torsional responses. The shift in the mean value is due to misalignment preloads.

Vibration waveforms and Fourier spectra for the second rotor (rotor-2) of the coupled rotor system are obtained (not shown here). For the case of rotor-2 also, the vibration amplitudes along horizontal direction are more compared to vertical direction for the reasons discussed earlier for the case of rotor-1. It may be noted that the overall vibration response depends on the excitation level and more so on the relative phase between misalignment excitation and unbalance. The unbalance at the discs of rotor-1 and rotor-2 are in same phase. However, the misalignment forces act in opposite directions on the two rotors. The minor differences in the vibration response of rotor-1 and rotor-2 are due to phase difference between unbalance and misalignment excitations. Depending upon the misalignment excitation phase with respect to unbalance phase angle, these excitations (i.e. unbalance and misalignment) can become fully additive to fully subtractive. However, it may be emphasized that the spectral character of the vibration response for both the rotors is found to be similar and hence the response data for rotor-2 is not shown here. Hence, the vibration response for misaligned rotors is discussed for rotor-1 for all subsequent cases.

Vibration responses at rotational speeds, $\omega = \omega_n/3 = 16.534$ Hz and $\omega = \omega_n/2 = 24.8$ Hz are shown in Fig. 9 for misaligned rotors ($dy = 0.32$ mm). Since the vibration response of both of the coupled rotors are similar; results are presented for rotor-1 only. At $\omega = \omega_n/3$ and $\omega_n/2$, the third and second harmonic of the rotational speed, respectively, matches with the first bending natural frequency and the subharmonic resonances are observed at these speeds. Axial and torsional vibration responses are similar to that at $\omega = \omega_n/4$ (Fig. 8), with strong 1*X* component along with noticeable but comparatively weaker 2*X*, 3*X* and 4*X* components. It may be noted that at $\omega = \omega_n/3$, the lateral vibrations (i.e. horizontal and vertical) are mainly 3*X*, with almost negligible 1*X* and 2*X* components. On the other hand, at $\omega = \omega_n/2$, 1*X* is quite noticeable in presence of strong 2*X*.

The full spectrum plot obtained using vibration data of vertical and horizontal vibrations shown in Fig. 10 for different rotor speeds; for $\omega = \omega_n/4$, $\omega_n/3$ and $\omega_n/2$. As mentioned earlier, apart from frequency contents and its magnitude, the full spectrum additionally reveals the whirl direction of the rotor motion at different harmonics. Amplitude levels of the spectral components are more compared to the rotor without misalignment (Fig. 7). Full spectrum in Fig. 10a shows first four harmonics of the rotational speed along positive (+ve) and negative (−ve) frequency axis. This suggests the parallel misalignment introduces backward whirling vibration motion as well. Figs. 10b and c show full spectra for $\omega = \omega_n/3$ and $\omega_n/2$, respectively. The figures reveal −ve frequency components with significant amplitudes, along with strong +ve frequency components. The vibration motion is forward whirling for all the harmonics. It may be noted that the 3*X* spectral component is quite stronger at $\omega = \omega_n/3$ compared to 2*X* frequency component at $\omega = \omega_n/2$; because of higher level of misalignment forces and moments associated with 3*X* harmonic than the 2*X* harmonic. The presence of strong 3*X* harmonic can be attributed to the three-pin configuration of the flexible coupling.

The presence of strong backward whirl frequency component, particularly at bending natural frequency component at integer fraction of critical speed is a significant finding related to the misalignment fault. The feature may be used to differentiate misalignment from other malfunctions such as crack, which also exhibit similar spectral characteristics in the single-sided spectra (i.e. conventional Fourier transform). Though the backward whirling frequency components are sufficiently strong, they are less compared to amplitudes of forward whirling frequency components. This means that the overall vibration motion is forward whirling for misaligned rotors. It may be noted that the synchronous vibration response

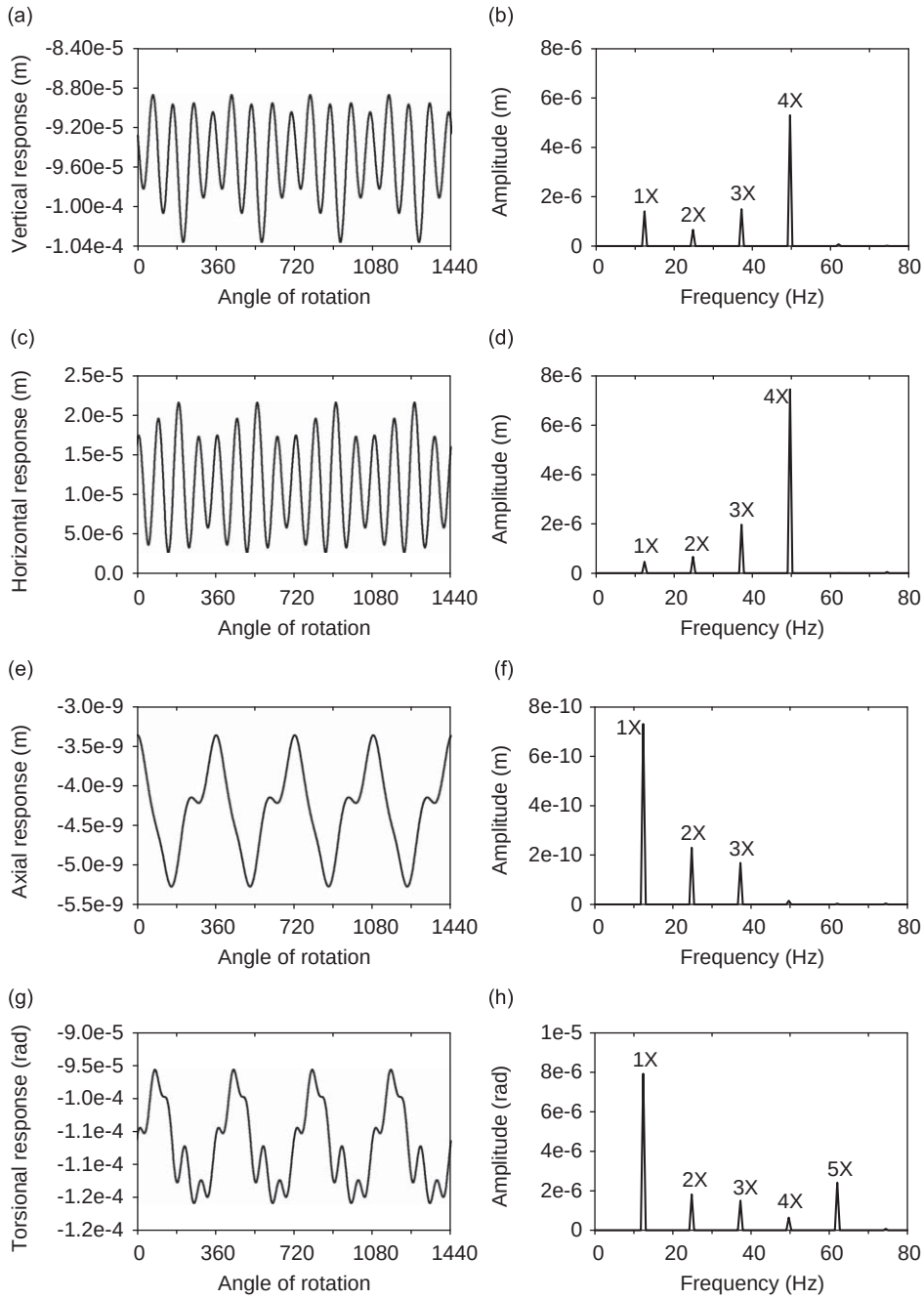

Fig. 8. Vibration response and its Fourier spectra of rotor-1 of misaligned rotors, dy = 0.32 mm, $\omega = \omega_n/4 = 12.4$ Hz.

for misalignment also involves strong backward whirling component ($-1X$) that was completely absent in the case of pure unbalance response (without misalignment) of the rotor system (Fig. 7).

The presence of backward whirling frequencies would result in elliptical orbit for the rotor centre as observed from the orbit plots of Fig. 11. Lesser the difference between +ve and −ve frequencies, lesser would be the minor axis diameter of the elliptical orbit and the orbit is stretched in one direction. When −ve and +ve frequency amplitudes become equal; the orbit becomes the straight line. Multi-looped orbit with stretch in the direction perpendicular to the misalignment direction is recommended as typical parallel misalignment vibration symptom. Orbits shown in Fig. 11 are multi-looped (four loops, three loops and two loops at $\omega = \omega_n/4$, $\omega_n/3$ and $\omega_n/2$, respectively). The rotor centre orbits are inner-looped and stretched in the lateral direction, nearly orthogonal to the misalignment direction. Cracked rotor vibration response also reveal

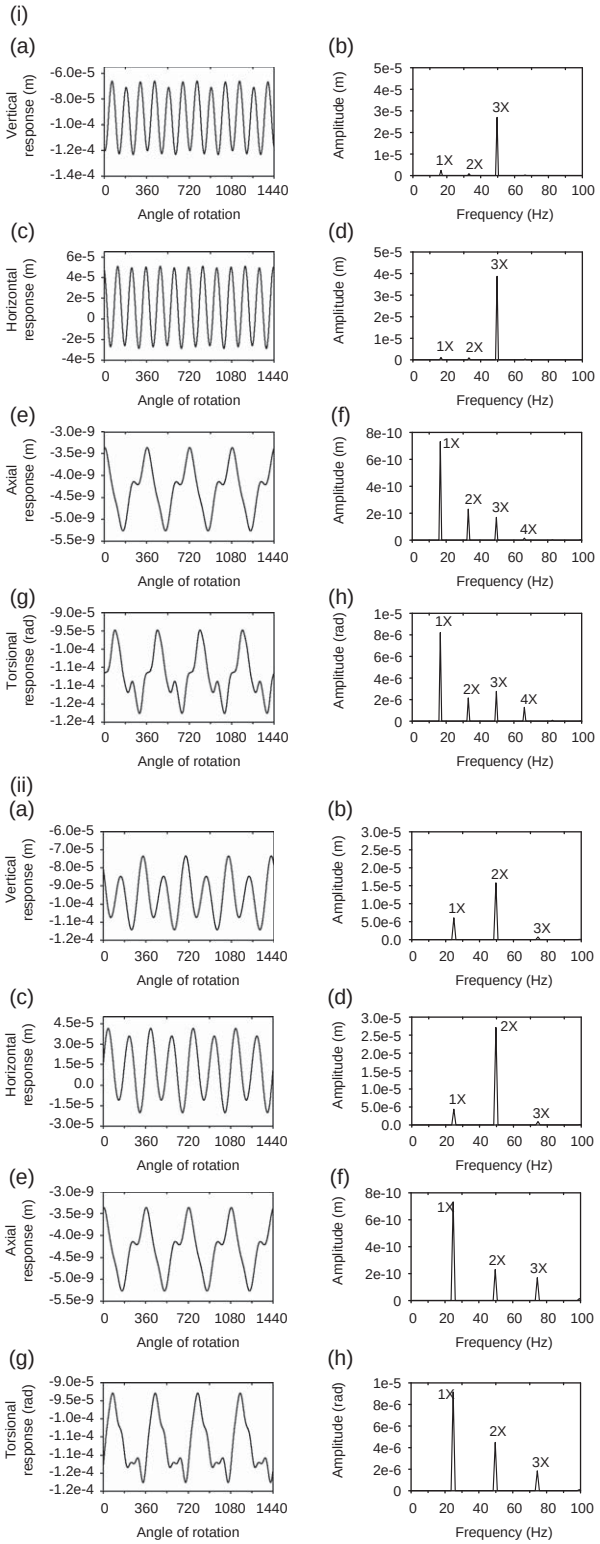

Fig. 9. Vibration response and its Fourier spectra of rotor-1 of misaligned rotors, dy = 0.32 mm: (a) $\omega = \omega_n/3 = 16.534$ Hz and (b) $\omega = \omega_n/2 = 24.8$ Hz.

similar type of inner-looped orbits, but the orbits are almost circular and not stretched [14]. As mentioned earlier, this stretch in the orbit along one direction is due to rotor's unequal effective stiffness mainly due to radial preload the misalignment exerts on the rotor.

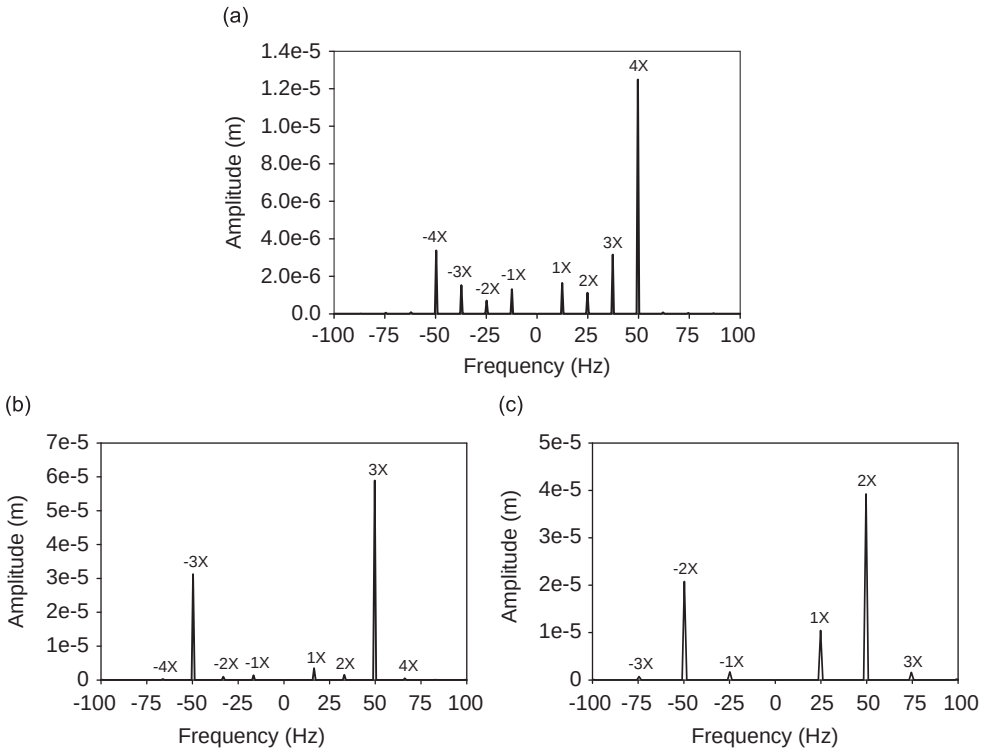

Fig. 10. Full spectra of vibration response of misaligned rotors, d$y = 0.32$ mm: (a) $\omega = \omega_n/4 = 12.4$ Hz, (b) $\omega = \omega_n/3 = 16.534$ Hz and (c) $\omega = \omega_n/2 = 24.8$ Hz.

Full spectra in Fig. 12 show that with increased level of misalignment (0.89 mm), the basic character of full spectrum plot is maintained with increased strength. The amplitudes of frequency components increase by about three times compared to those for lower level (d$y = 0.32$ mm, Fig. 10) due to increased misalignment excitation level. The strong backward whirling components at $-3X$ and particularly at $-2X$ at half the bending critical speed is an important feature for misalignment, although the overall whirl is still forward whirl.

4.3. Unbalance vibration response of coupled rotors with angular misalignment

Vibration response of the angularly misaligned coupled rotors is obtained from the FE model considering misalignment excitation forces and moments at the coupling location. The misalignment forces and moments are found using coupling stiffness coefficients. It may be noted from the Fourier spectrum plots of stiffness coefficients (Fig. 5b) that the stiffness coefficients vary periodically with each cycle of rotation. The stiffness coefficients exhibit harmonics of rotational speed, usually the first six. However, the 1*X*, 3*X* and then 2*X* frequency components are significant in amplitudes. Angular misalignment is considered in the vertical plane (about *Z*-axis). Since angular misalignment in the other direction would exhibit the similar dynamics of the system, it is not considered in the study.

Fig. 13 shows the vibration response in lateral, axial and torsional dof for rotational speed $\omega = \omega_n/4 = 12.4$ Hz. An angular misalignment value of 0.5° (i.e. $\beta = 0.5^\circ$) about horizontal direction is considered for the study. Lateral vibration response rich in spectral components (first five harmonics) with strongest 4*X* component along with strong 1*X* and 3*X* is observed. Here at $\omega = \omega_n/4$, fourth harmonic matches with the bending natural frequency of the rotors, hence, 4*X* harmonic is strongest in lateral vibrations. Vibration level in vertical direction is more than the horizontal direction due to increased effective stiffness in horizontal direction, as the induced misalignment is about horizontal direction.

Though the amplitude levels are small, the axial response (Figs. 13e and f) show significant 1*X*, 2*X* and 3*X* spectral components with 3*X* component being the strongest. It is important to recollect that the axial vibration with dominant 1*X* component in presence of other harmonics is observed for parallel misalignment case (Fig. 8). The presence of stronger 3*X* harmonic in the axial vibrations could be used to differentiate the type of misalignment present in the rotor (much smaller than 1*X* in parallel misalignment while much stronger than 1*X* in case of angular misalignment). The torsional response (Figs. 13g and h) clearly shows noticeable presence of harmonics up to order five. Odd harmonics in the frequency spectrum i.e. 1*X*, 3*X* and 5*X* are dominant. Presence of strong 5*X* can be explained due to excitation of torsional natural frequency (61.3 Hz) by the fifth-order harmonic (62 Hz) of the rotational speed. The torsional response in the case of parallel

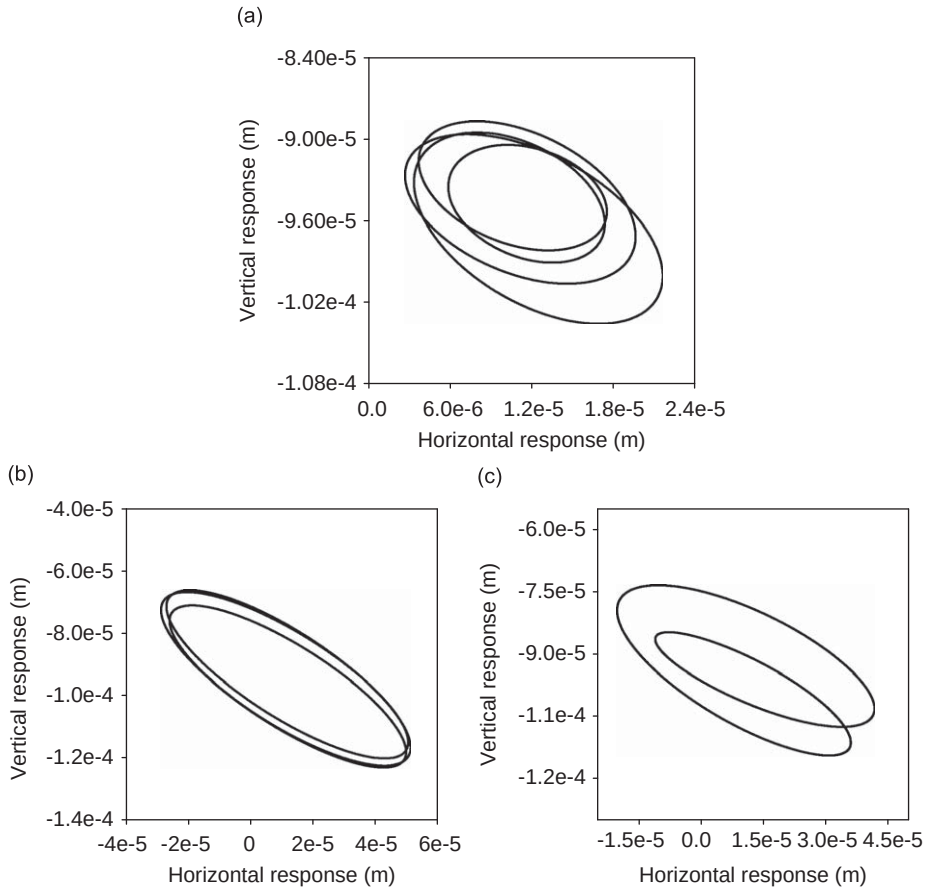

Fig. 11. Orbit plots for misaligned rotors, dy = 0.32 mm: (a) $\omega = \omega_n/4 = 12.4$ Hz (b) $\omega = \omega_n/3 = 16.534$ Hz and (c) $\omega = \omega_n/2 = 24.8$ Hz.

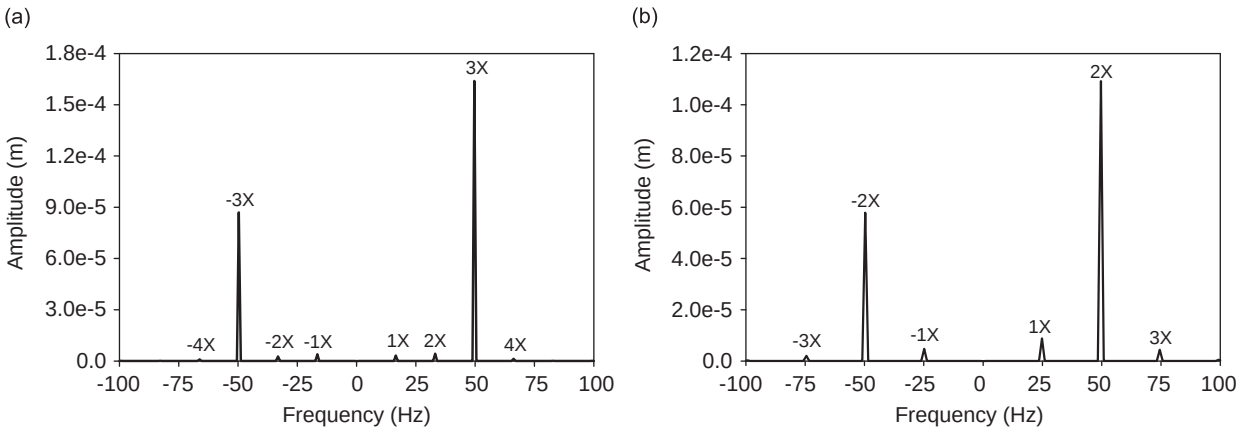

Fig. 12. Full spectra of vibration response of misaligned rotors with increased misaligned level, dy = 0.89 mm: (a) $\omega = \omega_n/3 = 16.534$ Hz and (b) $\omega = \omega_n/2 = 24.8$ Hz.

misalignment is dominated by 1*X* frequency component (Fig. 8h). However, as it is clearly evident from Fig. 13h, for angular misalignment, the 1*X* and 3*X* harmonics are strong and of comparable amplitudes. A strong 3*X* frequency component in torsional vibration is thus the distinguishing vibration feature in the case of angular misalignment. Horizontal, axial and torsional vibration waveforms have non-zero mean values because of misalignment preload. It may be noted that due to static sag, vertical waveform always have non-zero mean. Presence of non-zero mean for horizontal, axial and torsional vibrations can be considered as a misalignment symptom.

Fig. 14 shows the vibration response for $\omega = \omega_n/3 = 16.534$ Hz and $\omega = \omega_n/2 = 24.8$ Hz (for angular misalignment $\beta = 0.5^\circ$). Strong 3*X* vibrations are clearly observed in vertical, horizontal, axial and torsional responses at $\omega = \omega_n/3$. The 3*X* frequency component is many times stronger than 1*X* component. Strong 3*X* frequency in torsional and axial vibrations in particular is an important indicator of angular misalignment. As the third harmonic of rotational speed matches with the first bending natural frequency of the coupled rotors, presence of strong 3*X* harmonic in lateral vibrations is observed. For similar reason, vibrations in lateral directions experiences strong 2*X* motion at $\omega = \omega_n/2$. However, the 2*X* frequency component is weaker to 1*X* frequency along horizontal direction. Use of strong 2*X* vibration response as a misalignment symptom is questionable and should not be solely used for the misalignment diagnosis. At $\omega = \omega_n/2$, the axial and torsional vibrations also have strong 3*X* harmonic, along with 1*X* and 2*X* harmonics.

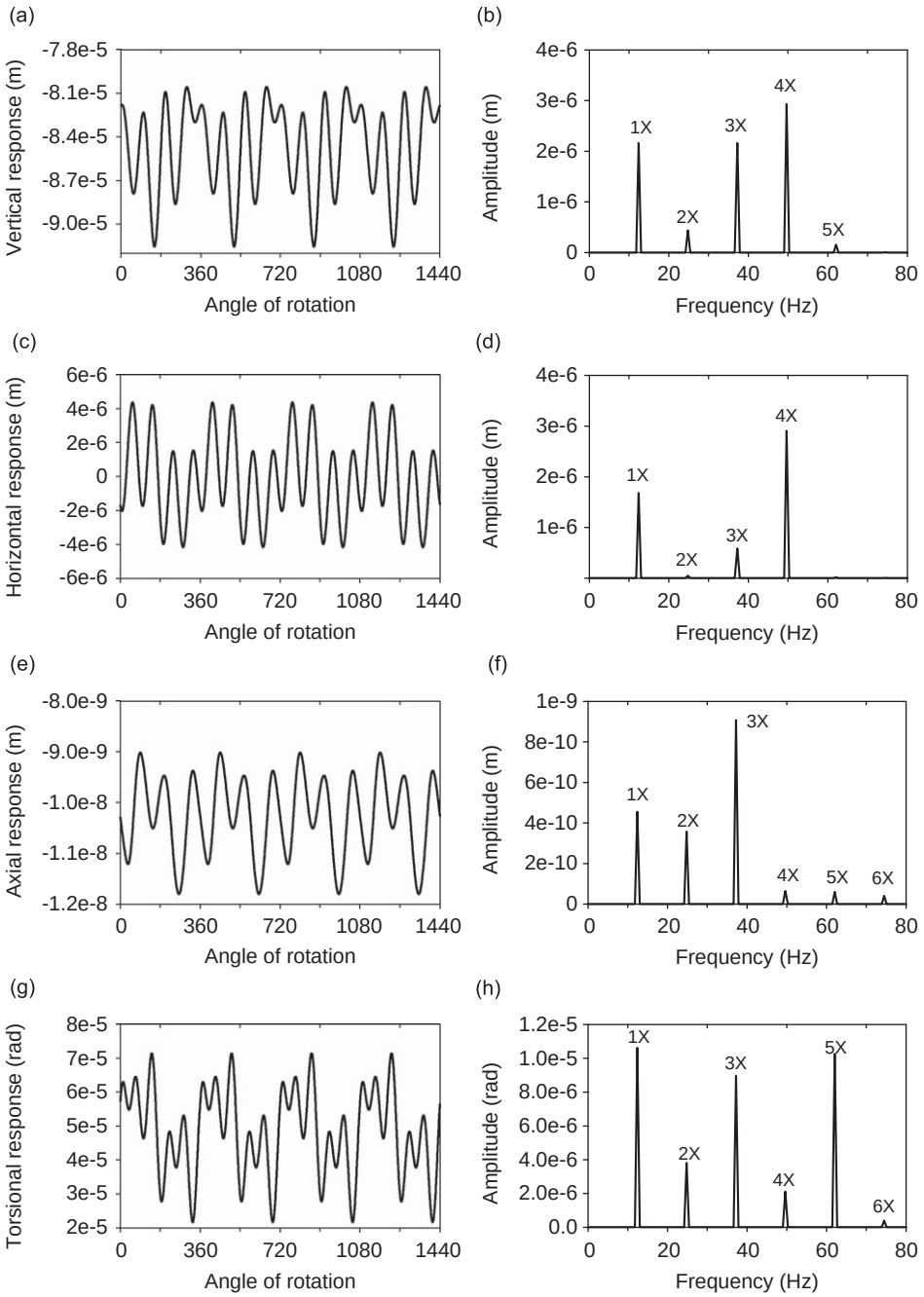

Fig. 13. Vibration response and its Fourier spectra of angular misaligned rotor, $\beta = 0.5^\circ$, $\omega = \omega_n/4 = 12.4$ Hz.

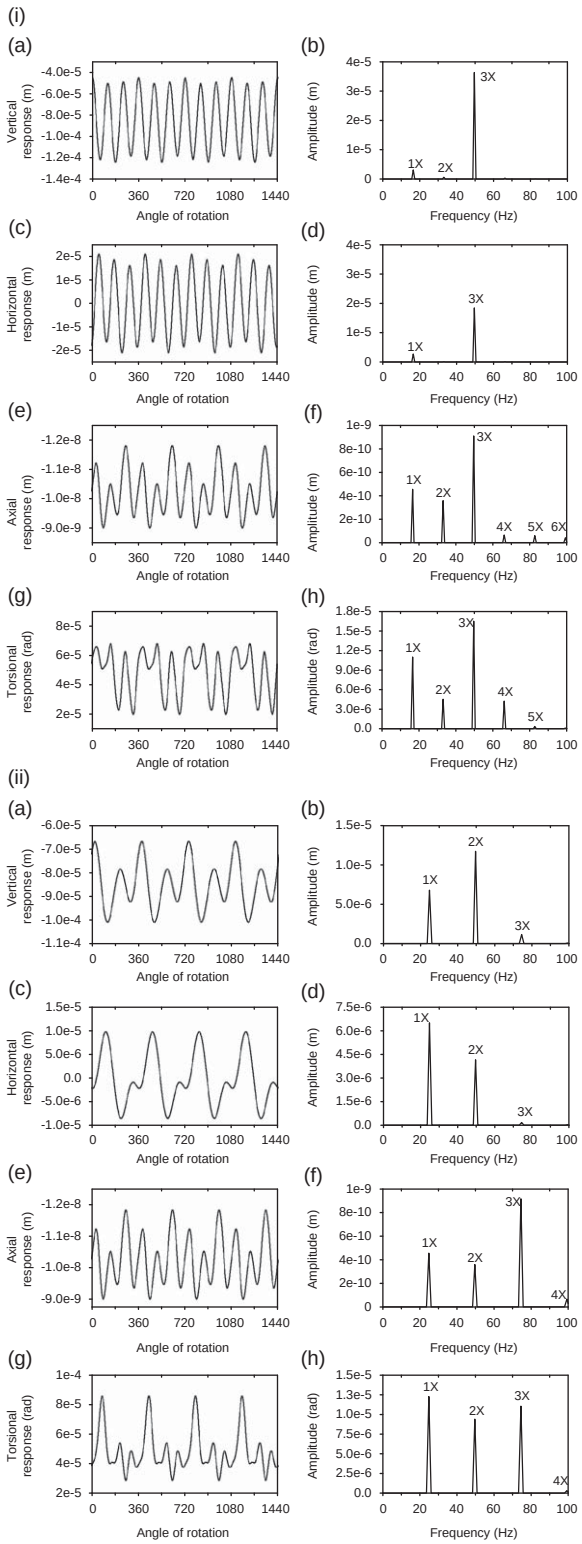

Fig. 14. Vibration response and its Fourier spectra of angular misaligned rotors, $\beta = 0.5^{\circ}$: (a) $\omega = \omega_n/3 = 16.534$ Hz and (b) $\omega = \omega_n/2 = 24.8$ Hz.

It may be emphasized here that the cracked rotor is known to exhibit 1*X* and 2*X* in its axial and torsional vibration response and 3*X* is almost non-existent [15]. This feature could be exploited in separating crack and misalignment response features.

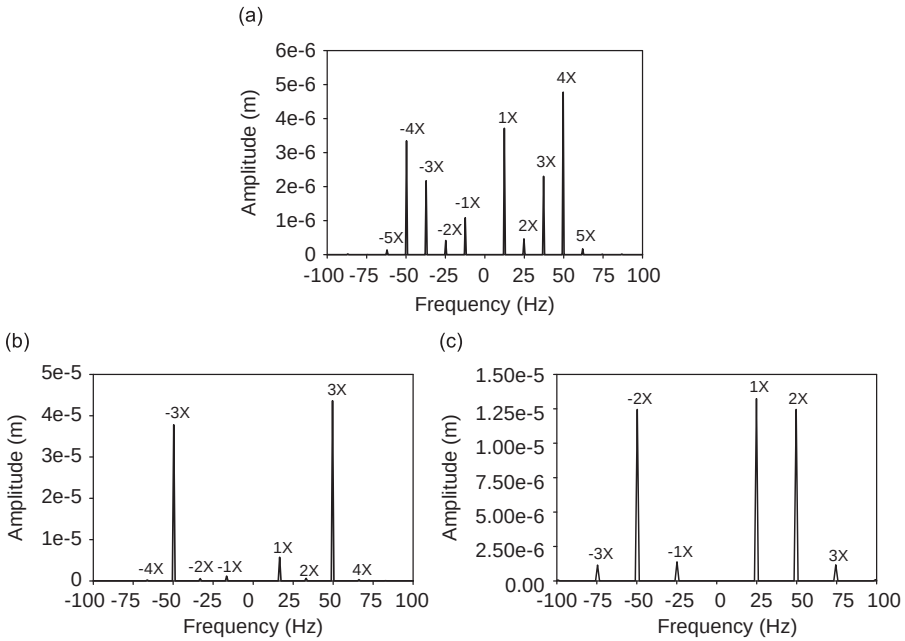

Fig. 15. Full spectra of vibration response of misaligned rotors, $\beta = 0.5^{\circ}$: (a) $\omega = \omega_n/4 = 12.4$ Hz, (b) $\omega = \omega_n/3 = 16.534$ Hz and (c) $\omega = \omega_n/2 = 24.8$ Hz.

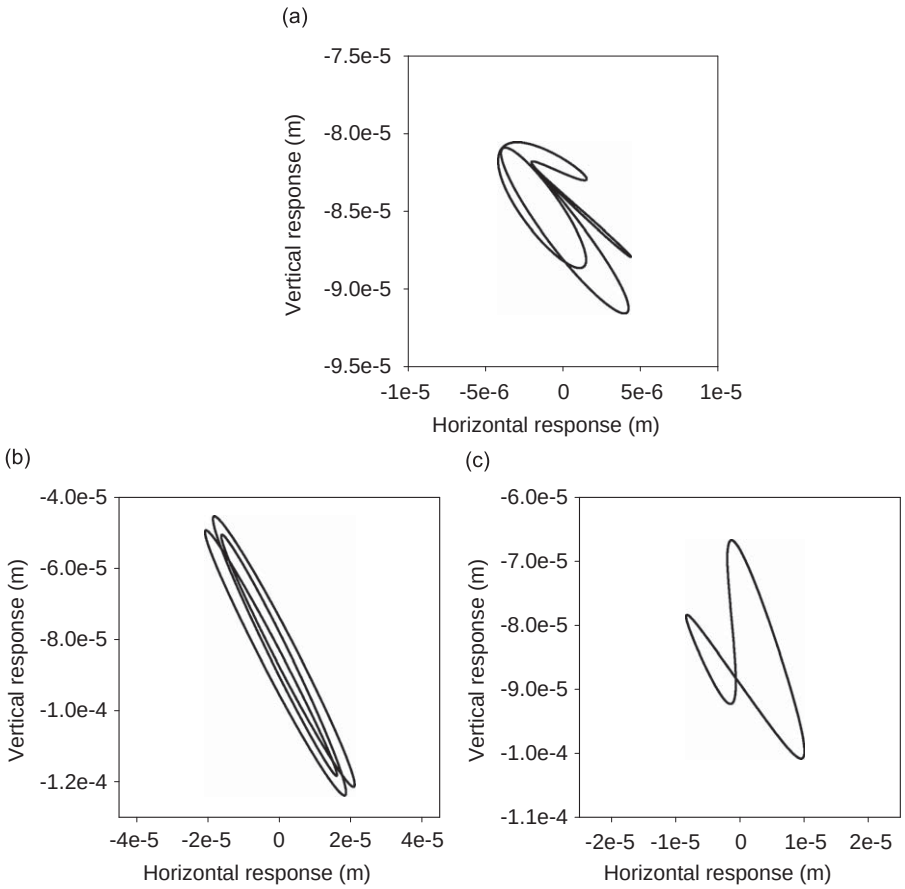

Fig. 16. Orbit plots of vibration response of angular misaligned rotors, $\beta = 0.5^{\circ}$: $\omega = \omega_n/4 = 12.4$ Hz, (b) $\omega = \omega_n/3 = 16.534$ Hz and (c) $\omega = \omega_n/2 = 24.8$ Hz.

Fig. 15 shows full spectra for $\omega = \omega_n/4 = 12.4$ Hz, $\omega = \omega_n/3 = 16.534$ Hz and $\omega = \omega_n/2 = 24.8$ Hz. Similar to parallel misalignment, spectral components along both $-ve$ and +ve frequency axes are present. Fig. 15a for $\omega = \omega_n/4$ shows that though overall vibration motion is forward whirling for each of the spectral component, the negative frequency components are sufficiently strong. Full spectra reveal strong 1*X*, 3*X* and 4*X* spectral components with weak 2*X* and 5*X* components. Amplitude of the 4*X* harmonic component is highest. At $\omega = \omega_n/3$, full spectrum plot (Fig. 15b) is dominated by strong 3*X* spectral component. Other harmonics are weak in comparison with 3*X*. The full spectrum for $\omega = \omega_n/2$ (Fig. 15c) shows strong 1*X* and 2*X* spectral components. Vibrations at 1*X* (i.e. synchronous motion) are strongly forward whirling. It may be further noticed that level of 2*X* frequency component is slightly less compared to 1*X*. $-2X$ and $+2X$ components are observed almost equal. Higher level of 1*X* vibrations is due to higher amplitude excitation forces at 1*X* frequency compared to those at 2*X* frequency.

Fig. 16 shows the orbit plot of angularly misaligned rotors (i.e. $\beta = 0.5^\circ$) for $\omega = \omega_n/4$, $\omega_n/3$ and $\omega_n/2$ indicating stretched orbits. Orbits are multi-looped (three loops at $\omega = \omega_n/3$ and two loops for $\omega = \omega_n/2$), stretched along vertical direction and exhibit, in general, outer loops. It has been shown that the orbit plot for parallel misaligned rotors (Fig. 16b) is clearly inner looped for $\omega = \omega_n/2$. The shape of rotor orbits could thus be used for diagnosis of rotor faults like crack, parallel misalignment and angular misalignment particularly at $\omega = \omega_n/2$. Orbits with two loops (inner loops) are observed for cracked rotors as well as rotors with parallel misalignment, however, the rotor orbit is stretched in one direction for parallel misalignment. In case of angular misalignment; outer looped orbit is observed (Fig. 16c).

It may be noted that with increase in the level of misalignment, the excitation level increases proportionately. Hence, as shown in Fig. 17, for higher angular misalignment of $\beta = 1.5^\circ$, similar spectral components with increased amplitudes appear in the spectra. The relative spectral distribution remains unchanged, indicating the full spectral features with strong backward whirl components can indeed be used and the increase in these levels reflect increasing level of misalignment. Comparison of Fig. 17 with Fig. 10 also indicates sensitivity of these spectral features to severity of the fault (level of misalignment).

5. Conclusions

In this work, the influence of types of misalignment on the rotor vibration behaviour is investigated in detail. In addition to the vibration waveforms, orbit plots and conventional one-sided Fourier transforms, two-sided spectrum (full spectrum) is effectively used to identify unique vibration features related to the misalignment fault. Based on the investigation made at sub-critical speed range, following conclusions are derived:

1. A new misalignment model using experimentally measured data on forces induced due to misalignment is proposed. The proposed model in the form of a novel stiffness matrix shows that for the case of the coupling considered, the majority of the misalignment forces induce higher harmonics and out of them, the 3*X* frequency component is more prominent. It may also be noted that the forces vary continuously during rotation with large mean force acting due to the misalignment. The model thus captures the dynamics of the coupling excitation on the rotor with accurate stiffness coefficients representing the coupling. Perhaps for the first time, the coupling stiffness matrix is systematically formulated that exhibits cross-coupled coefficients and hence indicates the possibility of coupled lateral–axial–torsional vibration response of the rotor due to the flexible pinned coupling. The misalignment excitation obtained after multiplying the formulated stiffness matrix with induced misalignment is applied as external nodal input force to the FE model of the coupled rotors.

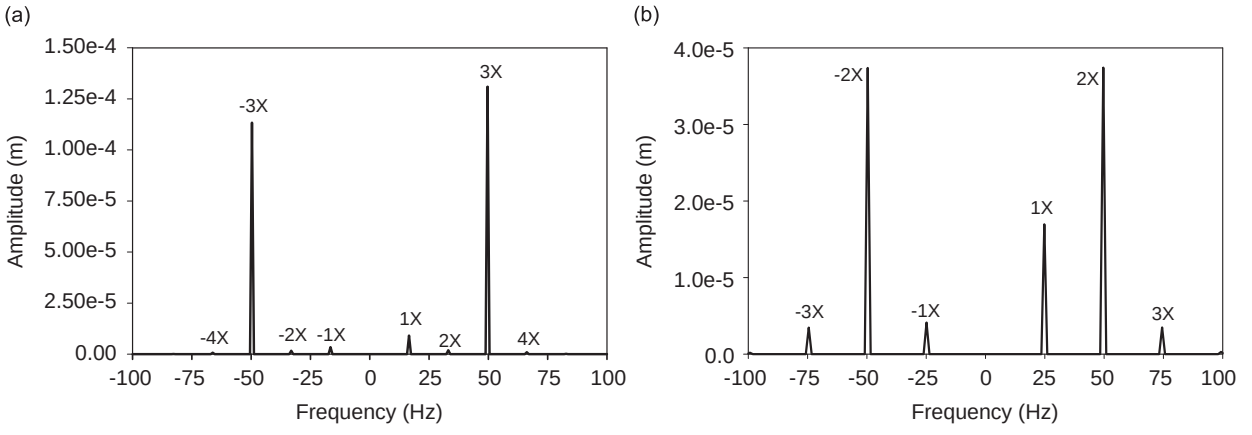

Fig. 17. Full spectra of vibration response of misaligned rotors for an increased level of misalignment, $\beta = 1.5^\circ$: (a) $\omega = \omega_n/3 = 16.534$ Hz and (b) $\omega = \omega_n/2 = 24.8$ Hz.

2. Lateral vibrations rich in harmonics of rotational speed are observed for both types of misalignment. The misalignment results in a major source of vibration if either of the harmonics (mainly the first six) i.e. an integer multiple of the rotational speed matches with the bending natural frequency of the rotor system generating subharmonic resonances.
3. The misalignment (parallel and angular both) in the rotor system reveals strong levels of backward whirling (negative) frequencies in the full spectrum plot. Although the vibration of the misaligned rotors is in effect forward whirling (due to $+nX > -nX$), the presence of strong $-$ve frequency components in the vibration response of the misaligned rotor is an important observation for the diagnosis of misalignment. The presence of strong $-$ve higher harmonic frequency components are strong contenders for unique identification features of rotor misalignment and hence can distinguish misalignment from rotor crack as the later generates very weak $-$ve frequency components.
4. Multi-looped (three loops at $\omega = \omega_n/3$ and two loops for $\omega = \omega_n/2$) and stretched orbits are typical misalignment fault indicators. Rotors with parallel misalignment reveal inner looped orbits, where as rotors with angular misalignment exhibit outer looped orbits. This is an important feature which can be used along with the full spectra to identify type of misalignment present in the system.
5. Coupling of bending–torsional–axial vibrations are observed in the response of the misaligned rotors. Coupling of all three motions is established for the first time in the case of misaligned rotors. Higher harmonics in the axial and torsional responses are observed. Irrespective to the rotational speed, parallel misalignment reveals stronger $1X$ axial and torsional responses while the higher harmonics are relatively weak. On the other hand, an angular misalignment exhibits very strong $3X$ harmonic component in its axial and torsional vibration response at 1/3rd critical speed. This difference in the frequency composition of the axial and torsional responses could also be very useful in differentiating the type of misalignment present in the system. The torsional vibration spectrum also distinguishes between crack and misalignment as the crack typically does not generate significant $3X$ frequency component in torsional vibration at 1/3rd critical speed. While these features are different for parallel and angular misalignment, the strong $-$ve frequency components in full spectra for both parallel and angular misalignments ensure that irrespective of the type of misalignment one can detect misalignment fault in a rotor bearing system with these unique features of full spectrum. More work on different types of couplings is currently underway.

Acknowledgements

The authors gratefully acknowledge financial assistance received for the study from the Department of Science and Technology, Government of India (no. SR/FTP/ETA-08/2003).

References

[1] C.B. Gibbons, Coupling misalignment forces, *Proceedings of the Fifth Turbomachinery Symposium*, Gas Turbine Laboratory, Texas A & M University, TX, 1976, pp. 111–11306.
[2] A.S. Sekhar, B.S. Prabhu, Effects of coupling misalignment on vibration of rotating machines, *Journal of Sound and Vibration* 185 (1995) 655–671.
[3] H.P. Bloch, F.K. Geitner, *Practical Machinery Management for Process Plants 2, Machinery Failure Analysis and Troubleshooting*, Gulf Publishing Company, Houston, TX, 1986.
[4] M. Xu, R. Marangoni, Vibration analysis of a motor-flexible coupling-rotor system subjected to misalignment and unbalance—part I: theoretical model and analysis, *Journal of Sound and Vibration* 176 (1994) 663–679.
[5] I. Redmond, K. Al-Hussain, Misalignment as a source of vibration in rotating shaft systems, *Proceedings of IMAC Conferences IMAC19*, 2000, pp. 116–123.
[6] K.M. Al-Hussain, I. Redmond, Dynamic response of two rotors connected by rigid mechanical coupling with parallel misalignment, *Journal of Sound and Vibration* 249 (2002) 483–498.
[7] G. Catania, A. Maggiore, Dynamic behaviour of flexible mechanical couplings under general misalignment condition, *ASME International Mechanical Engineering Congress and Exposition* November (2004) 431–438.
[8] A.W. Lees, Misalignment in rigidly coupled rotor, *Journal of Sound and Vibration* 305 (2007) 261–271.
[9] D.L. Dewell, L.D. Mitchell, Detection of a misaligned disk coupling using a spectrum analysis, *Journal of Vibration, Acoustics, Stress and Reliability in Design* 106 (1984) 9–16.
[10] J. Piotrowski, *Shaft Alignment Handbook*, Marcel Dekker Inc., New York, 1995.
[11] P.N. Saavedra, D.E. Ramirez, Vibration analysis of rotors for the identification of shaft misalignment—part I: theoretical analysis, *Proceedings of IMechE, Journal of Mechanical Engineering Science* 218C (2004) 971–985.
[12] P. Goldman, A. Muszynska, Application of full spectrum to rotating machinery diagnostics, *Orbit First Quarter* (1999) 17–21.
[13] W. Fengqi, G. Meng, Compound rub malfunctions feature extraction based on full spectrum cascade analysis and SVM, *Mechanical Systems and Signal Processing* 20 (2006) 2007–2021.
[14] T.H. Patel, A.K. Darpe, Vibration response of a cracked rotor in presence of rotor–stator rub, *Journal of Sound and Vibration* 317 (2008) 841–865.
[15] A.K. Darpe, K. Gupta, A. Chawla, Coupled bending longitudinal and torsional vibrations of a cracked rotor, *Journal of Sound and Vibration* 269 (2004) 33–60.